OPEN

Volcanic conduit migration over a basement landslide at Mount Etna (Italy)

I. Nicolosi[1], F. D'Ajello Caracciolo[1], S. Branca[2], G. Ventura[1] & M. Chiappini[1]

[1]Istituto Nazionale di Geofisica e Vulcanologia, via di Vigna Murata 605, 00143 Roma, Italy, [2]Istituto Nazionale di Geofisica e Vulcanologia, Osservatorio Etneo, Piazza Roma 2, 95125 Catania, Italy.

Correspondence and requests for materials should be addressed to G.V. (guido.ventura@ingv.it)

The flanks of volcanoes may slide in response to the loading of the edifice on a weak basement, magma push, and/or to tectonic stress. However, examples of stratovolcanoes emplaced on active landslides are lacking and the possible effects on the volcano dynamics unknown. Here, we use aeromagnetic data to construct a three-dimensional model of the clay-rich basement of Etna volcano (Italy). We provide evidence for a large stratovolcano growing on a pre-existing basement landslide and show that the eastern Etna flank, which slides toward the sea irrespective of volcanic activity, moves coherently with the underlying landslide. The filling of the landslide depression by lava flows through time allows the formation of a stiffness barrier, which is responsible for the long-term migration of the magma pathways from the coast to the present-day Etna summit. These unexpected results provide a new interpretation clue on the causes of the volcanic instability processes and of the mechanisms of deflection and migration of volcanic conduits.

The lithology and structure of the basement underlying active volcanoes play an important role in promoting flank instability, gravity sliding, volcanic spreading[1,2]. Therefore, the knowledge of the basement morphology is of primary importance to better understand the deformation field of active volcanoes and evaluate the associated hazard[3]. Because of the difficulty in collecting data on the basement morphology, which is commonly masked by the growth of the overlying volcanic successions, most structural and physical models of volcanoes appear to be poorly constrained, and a simple geometry is generally assumed (e.g., flat surface, with a constant slope, or with a step)[4–6]. This limits our knowledge of the processes (e.g., sliding) affecting the basement and the understanding of the effects of such processes on the overlying volcanoes. Here, we use aeromagnetic data to reconstruct the geometry of the non-magnetic surface underlying the Etna active volcano (3328 m a.s.l., Italy), which is affected by a seaward sliding of its eastern flank. The Etna sedimentary basement mainly consists of clay-rich rocks and shows an asymmetric topography with a wide depression located below the eastern flank of the edifice[7]. However, the basement geometry above 1200 m a.s.l. and inside the depression is poorly known because of the lack of available data[7]. The polygenetic composite structure of Etna develops on the unstable continental margin of eastern Sicily in the last 220 ka as consequence of an extensional tectonics that favoured the formation of a primitive lava-shield along the NNW-SSE striking Timpe fault system[8] (Fig. 1a). The gradual shifting of the shallower feeder system from the coastal sectors towards NNW at about 130 ka[7,8], and the change from a fissural to a central type activity, lead to the formation of the earlier stratovolcano at about 110 ka in the Valle del Bove area[8]. A further NNW shift of the feeder system in the last 60 ka is responsible for the building of the present-day edifice[7,8]. The Etna eastern flank is affected by a southeastward sliding (Fig. 1a)[9–11]. The northern boundary of the sliding sector is represented by the NE rift fissure network and by the left-lateral Provenzana-Pernicana fault system. The southern boundary is defined by the right-lateral Tremestieri-Trecastagni fault system and by the hidden Belpasso-Ognina fault[9,11]. These faults depart from the summit craters and propagate down to the Ionian coast depicting a horseshoe-like shape. The central and downslope sector of the Etna sliding flank is affected by the Timpe seismogenic faults, which also move aseismically by an almost continuous creep along the Ionian margin (Fig. 1a)[12]. Geodetic data reveal that the dynamics of the Etna unstable flank is characterized by sudden accelerations related to magma intrusions and by a fairly constant ESE sliding (about 0–30 mm/yr) and subsidence (about 3–20 mm/yr) irrespective of the eruptive activity[9]. In the central coastal sector of the volcano, the subsidence is larger than 5 mm/yr (Fig. 1a). The Etna western and northern sectors show a deformation field characterized by a roughly radial horizontal pattern related to inflation/deflation dynamics. This deformation field, which departs from the central crater, is consistent with magma intrusions at shallow depth. A morphological bulge including Miocene-Pleistocene carbonate terrains and folded Plio-Quaternary sediments characterizes the offshore Ionian margin of the volcano (Fig. 1a)[13]. The bulge is affected by landslide scars, gravity slides and mass wasting related to the gravity instability of the continental offshore[6].
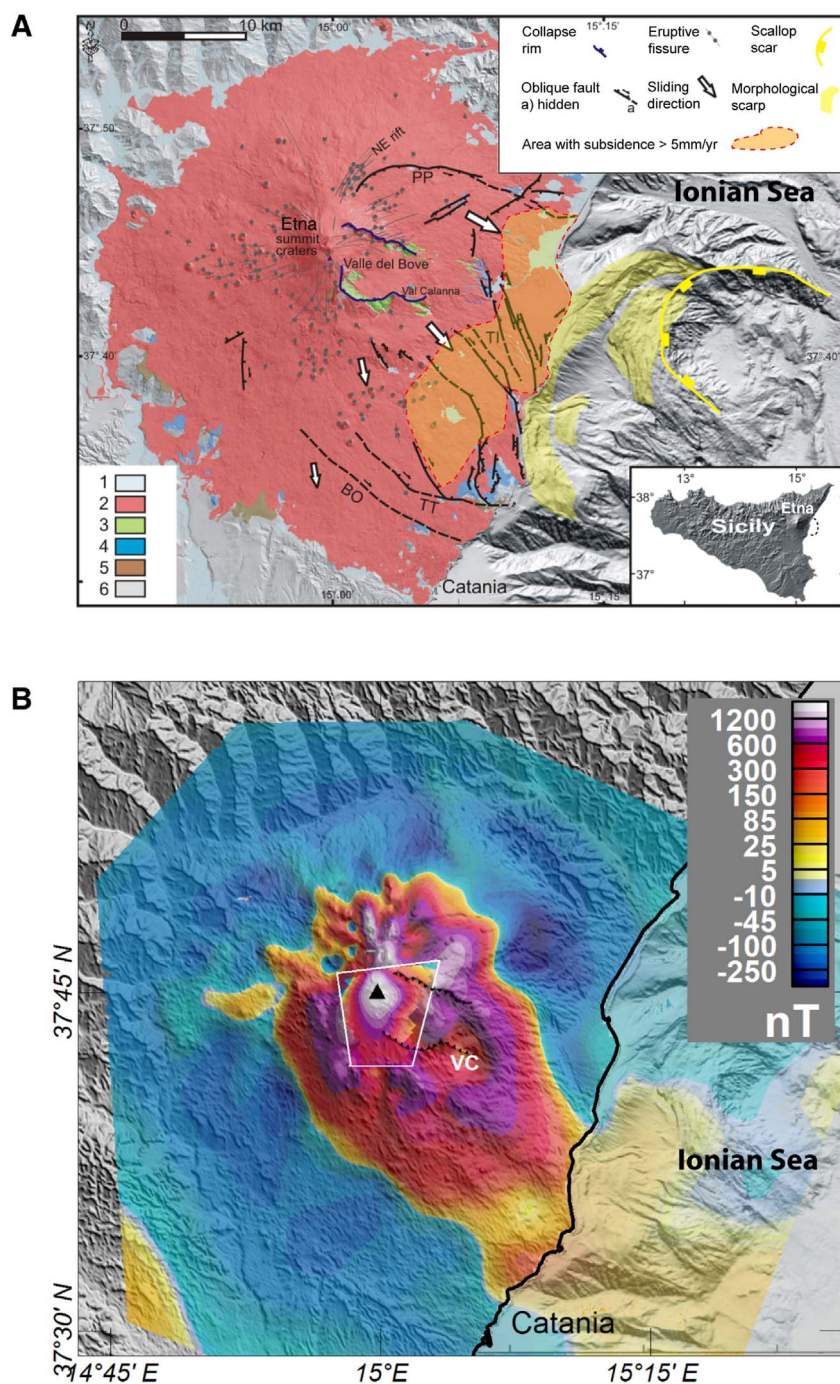
Figure 1 | (A) Geological and structural sketch map of the Etna volcano and its offshore sector with the main morphostructural features affecting the continental margin[6,7]. Legend: 1) present and recent alluvial deposits; 2) volcanics of the stratovolcano phase (60 ka – Present): 3) volcanics of the Valle del Bove phase (110–60 ka); 4) volcanics of the Timpe phase (220–110 ka); 5) volcanics of the Basal Tholeiitic phase (500–330 ka); 6) Sedimentary clay basement. Fault systems: PP = Provenzana-Pernicana; TI = Timpe; TT = Tremestieri-Trecastagni; BO = Belpasso-Ognina. The area of subsidence has been delimited from Permanent Scatterers analysis[9]. (B) Reduced to Magnetic Pole (RTP) magnetic anomaly map of Etna at 2200 m a.s.l.; the area enclosed by the white line contains the magnetic anomaly at 3500 m a.s.l. (Methods). Black triangles lines defines the Valle del Bove boundaries; VC = Val Calanna. Figure generated with AdobeIllustrator, AdobePhotoshop, and Irfanview.

Results

A high resolution aeromagnetic survey of Etna has been carried out in 2012. The details of the survey and the analytical methods are in Methods and Supplementary Figure S1. In order to correlate the magnetic anomalies with their sources, we applied the Reduction to the Magnetic Pole transformation (RTP) to the measured magnetic anomaly data. We construct a 3D model of Etna inner structure using the inversion algorithm described in Methods. The modelling

strategy is aimed to map the Etna magnetic bottom, which, according to the available intensity data on lava flows and clays[14,15], may represent the interface between the volcanic rocks and the non-magnetic basement. The available magnetization intensity values of lavas cluster between 5 and 13 A/m. Taking into account the distance between the magnetic sources and the airborne sensor as well as the relative compositional homogeneity of the Etna products, we consider the internal magnetization variations as mainly due to the volcanic pile.

As a result, we assume that (a) a bulk magnetization of the volcano describes the observed aeromagnetic signature, and (b) the main magnetization contrasts are described by thickness variations of the Etna volcanic succession. Under these assumptions, we explore different magnetic inversion models. A bulk magnetization value of 8 A/m minimizes the RMS error on the data and the difference between borehole data[7] and the modelled magnetic bottom (Methods).

The collected data evidence that the Etna magnetic signature does not relate to the present topography with the exception of the summit, which is characterized by a thicker volcanic pile and a higher concentration of vents (Fig. 1b). The magnetic anomaly has a NNW-SSE elongated sub-elliptical shape bounded to the east by the Timpe fault system, and may be divided in two main sectors (Fig. 1b): a northwestern sector departing from the summit craters and characterized by a high frequency pseudo-radial pattern, and an about 40 km long and 20 km wide southeastern sector, which is dominated by longer wavelengths. This latter extends from the Etna summit to the Ionian Sea. The radial pattern of the northwestern sector may mirror, according to deformation data[9], the radial dikes intruded in the upper northern and western flanks of the edifice. In the Etna southeastern magnetic sector, some short wavelength anomalies occur. These are characterized by linear and arcuate shapes; the most evident magnetic feature is the presence of a lower magnetized area located above Val Calanna where a deeply hydrotermalized dike swarm crops out[16]. This magnetic feature overlays a part of the well-known high velocity (Vp) and density body inferred by seismic and gravity data[17,18], which is poorly magnetized.

The results of the 3D modelling (Fig. 2a) show that thin volcanic products blanket the downslope topography of the northern, western and southwestern Etna flanks, whereas the southeastern flank is characterized by a huge, NNW-SSE elongated depressed area filled by up to 1000 m thick magnetized volcanic rocks (Fig. 2b). This depression extends from the summit craters to the Ionian Sea with an average slope of 7–8° (Fig. 2a, b). The western boundary of the depression is located below the Etna summit, where an eastern to
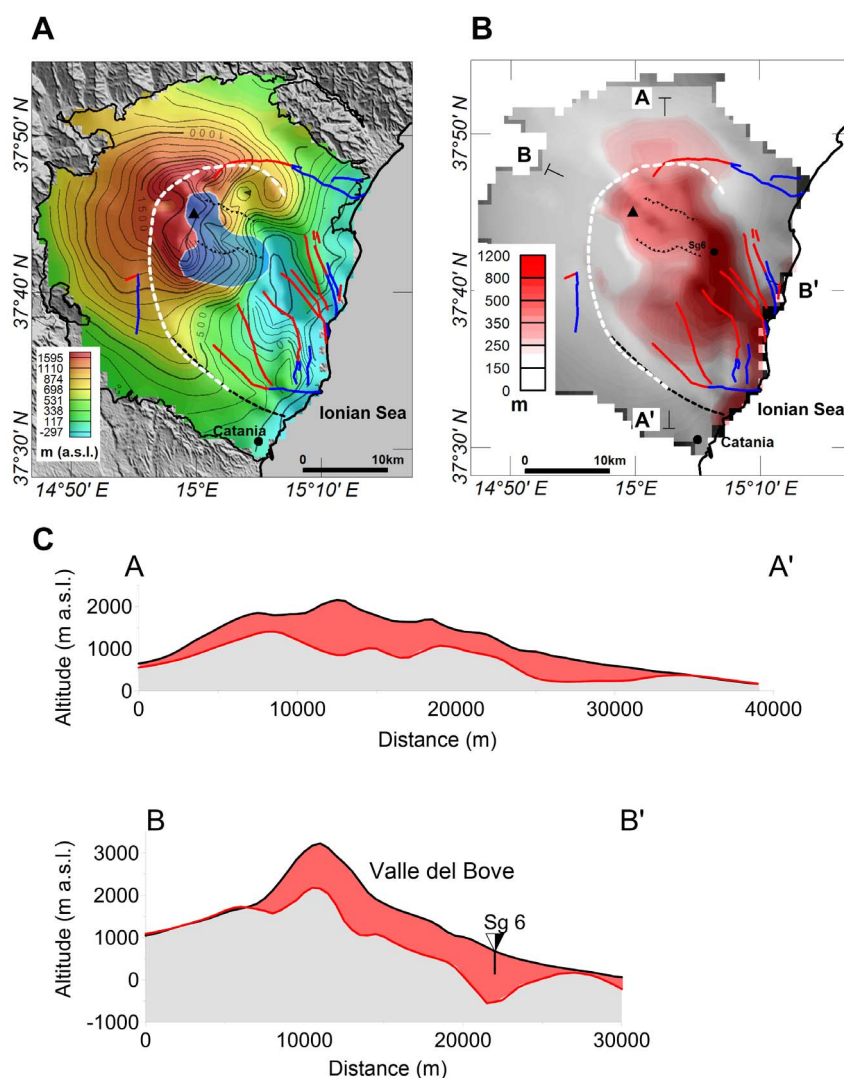

Figure 2 | (A) Modelled magnetic basement using a bulk magnetization value of 8 A/m. The isolines are 100 m spaced and refer to the altitude above the sea level (a.s.l.). The overall morphology describes a horse-shoe structure with a central depressed area and opened toward the sea. The light blue area represents the high velocity body at the sea level as imaged by seismic tomography[17]; red lines: seismogenetic faults; blue lines: creep faults[12]; black dashed line: Belpasso-Ognina blind fault; black triangles lines: morphological boundaries of Valle del Bove; white dashed line: morphological boundary of the landslide deduced from the magnetic modelling. (B) Map of the magnetized volcanic rocks thickness (in m). Sg6: borehole location[7]. The traces of the sections A-A' (NW-SE) and B-B' (N-S) in Fig. 2C) are also reported. (C) Sections A-A' and B-B' of the model reported in Fig. 2B: Grey = non-magnetic basement; red = magnetized volcanic rocks. The B-B' section shows that the Etna volcanic rocks fill a pre-existing depression. Figure generated with AdobeIllustrator, AdobePhotoshop, Oasis, and Irfanview.

southeastern facing main scarp is recognized. Below the Valle del Bove area, the magnetic bottom shows a convex up surface. Such surface overlaps the shallower portion of a solidified intrusive body recognized by seismic tomography (Fig. 2a)[17]. Two main arcuate escarpment slopes define the southern and northern boundaries of the depression (Fig. 2a). They enclose a large part of the present-day unstable eastern flank of the volcano (Fig. 1a).

Discussion and conclusions

The geometry of the eastern Etna non-magnetic basement is fully consistent with that of huge, east facing landslide depression pre-existing the construction of the volcano[7]. This latter conclusion is supported by the occurrence of 220 to 130 ka old, 10 to 30° west-dipping lava successions along the Ionian coast[8,21]. These lavas fill a depression located to the west of the present-day coastline. The overlying, 35 ka old lava flows dip towards the east, so excluding possible tilting due to fault activity[8,21]. The crown zone of the recognized landslide inferred by the magnetic modelling is below the summit area, where it is partly masked by the present-day shallower feeder system, and below the NE rift and Provenzana fault segment. The northern escarpment slope of the landslide does not coincide with the Pernicana fault, which represents the northern boundary of the unstable Etna flank (Fig. 2a). This is due to the superimposition of gravity-induced stress and magma-induced pressure at the northern tip of the NE rift[19]. The basement escarpment slope delimiting the southern boundary of the landslide partly overlaps the Tremestieri-Trecastagni and the hidden Belpasso-Ognina faults (Fig. 2a). The basement depression affects the lower, eastern and southeastern flanks of Etna including the shallowest portion of the Timpe faults, whose aseismic creep is driven by the fairly constant ESE sliding of

the unstable flank; the tectonic earthquakes associated to these faults are responsible for the discontinuous, short-lived co-seismic deformation[12]. The landslide model we propose is consistent with the seaward sliding of the Etna eastern flank regardless of volcanic activity and the aseismic, gravity-induced creep along the fault segments near the coast. These deformation features cannot be explained, according to results from GPS, InSAR[9] and physical models[20], by the weight of the volcanic pile and/or by an increase of magma pressure alone, but are signs of the general instability of the Ionian continental margin[6], as also confirmed by the higher values of subsidence concentrated along the central coastal sector of the volcano[9]. Such instability affects the clay-rich basement below Etna, whose eastern flank moves passively on a pre-existing sliding surface. The occurrence of a large landslide below Etna allow us to explain the northwestward migration of the volcanism during the past 220 ka, which started along the Ionian coast, and moved to the Valle del Bove area and present-day summit through time[8,21] (Fig. 3). According to models of magma ascent in the crust[22,23], a dike propagating within a low stiffness rock, i.e. clay, tends to deflect and form a sill when it encounters a higher stiff rock, e.g. lava flows. At Etna, the 220 ka old Timpe phase of activity started along the Ionian margin of the volcano by ascent of dikes crossing the low stiffness clay. As the Timpe lava flows pile filled the base of the landslide depression, a stiffness-related barrier developed, and the magma followed a deflected trajectory, possibly forming a sill (Fig. 3). Magma ascent is allowed at the northwestern tip of the sill, in a zone where only clay outcrops, i.e. in the middle/upper sector of the landslide. Here, the Valle del Bove phase of activity started at about 110 ka. When also this last sector of the landslide depression was filled by lava flows, a new sill forms, and, following the same mechanism, the youngest volcanic phase started
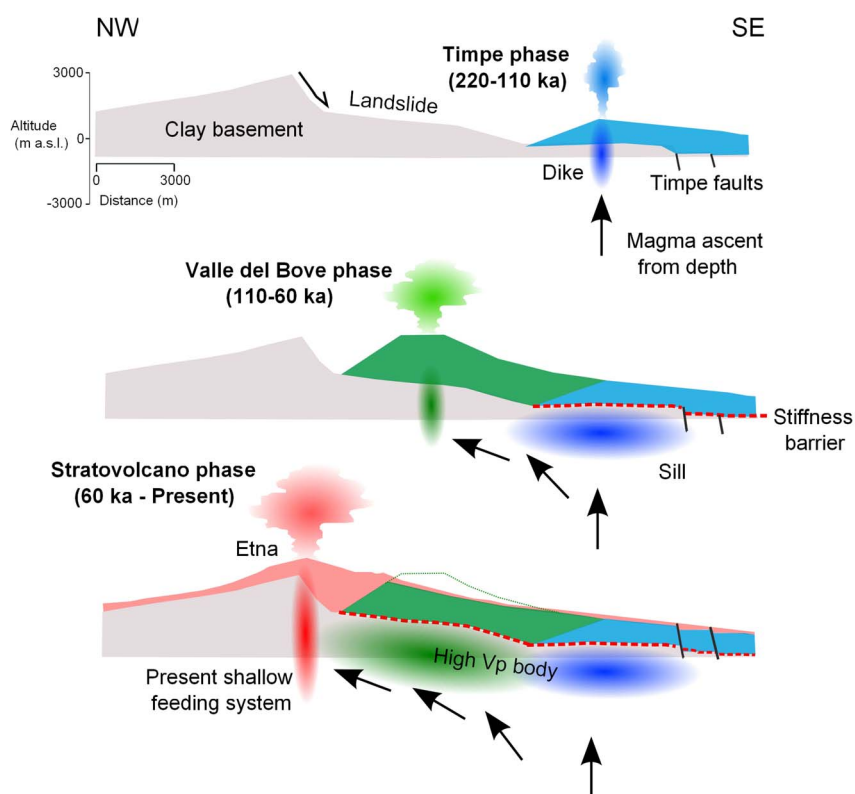

Figure 3 | Schematic model of the volcanism-landslide relationships at Etna volcano (from the top to bottom) depicted along a NW-SE profile crossing the Etna summit. The early activity (Timpe phase) develops at the base of a landslide depression (top). The filling of this depression by lava flows creates a stiffness barrier and a sill forms. The successive activity (Valle del Bove phase) occurs in a sector located to the northwest of the Timpe conduits (middle). Also in this latter case, a sill forms because of the development of a stiffness barrier. The last activity (stratovolcano phase) occurs northwest of the Valle del Bove conduits/sill(s) (bottom). The present-day Etna volcano growths during this last phase. The locations of the present shallow feeding system and of the high Vp body are from dynamic tomography studies[17]. Figure generated with Inkscape and Irfanview.

about 60 ka in the area where the basement reaches its maximum height, i.e. below the present Etna summit (Fig. 3). This interpretation is supported by dynamic tomography studies[17], which reveal the occurrence of a sill-like body with a high Vp anomaly between 1 and 3–4 km depth. This body has been interpreted as solidified intrusions laterally extending from the Etna summit to Valle del Bove and the lower, eastern flank[17]. According to our model, these intrusions could represent the sills formed during the Timpe and Valle del Bove phases of activity (Fig. 3). A low Vp/Vs anomaly at 1 km depth has been detected below the central craters during the recent activity. This anomaly evidences the current upward magma migration along vertical dikes[17]. Also, high Vp/Vs anomalies at 1 to 4 km depth beneath the eastern and southeastern Etna flanks have been recognized during the present eruptive activity[17]. These anomalies reflect the upraise of fluids from a deeper zone, suggesting, according to our model, the occurrence of a deeper plumbing system located southeast from the present Etna summit.

Our results highlight how the presence of active landslides below volcanic edifices and continental margin instability processes may influence the deformation field of active volcanoes and the migration of the shallower feeding systems. We conclude that the effects of a moving basement on the overlying volcanic edifice include: flank sliding irrespective of volcanic activity, subsidence at the base of the edifice, aseismic faulting, and relocation of the shallower conduit system. The approach used in this study should be extended to other volcanoes to better constrain physical and geological models of volcano deformation and to evaluate the hazard related to continental margin slope instability processes.

Methods

A high resolution aeromagnetic survey of Mount Etna volcano has been carried out by the Istituto Nazionale di Geofisica e Vulcanologia (INGV) during May 2012 acquiring about 3600 km of linear profiles. The use of a base station allowed the magnetic diurnal variation correction of the aeromagnetic dataset. The measured dataset was reduced to 2012.5 geomagnetic epoch. The anomaly values were obtained by subtracting the calculated main field component of the Earth's Magnetic Field from each diurnally corrected survey point using the 11th generation of the International Geomagnetic Reference Field (IGRF) model. Two aeromagnetic surveys at different altitudes have been conducted with the aim to take into account the large topographic variations of Etna. The aeromagnetic profiles are oriented N80°E and the line spacing is 1 km; one survey was flown at the altitude of 2200 m over the Etna region excluding the summit area, whereas the second survey covered the summit at about 3500 m of altitude. We applied the Reduction to the Magnetic Pole transformation (RTP) to the residual magnetic anomaly data using magnetization directions parallel to the present Earth's Magnetic Field (magnetic Inclination = 53°, magnetic Declination = 2.6°, modeled using IGRF) following[24]. The main purpose of this study was to calculate a 3D model of the Etna magnetic bottom. Our modeling was obtained starting from a magnetic source volume discretized by a single layer of cubic cells (2 km side), whose magnetization intensity is unknown. The top of this layer coincides with the Etna topographic surface. The topography is taken by NASA Shuttle Radar Topographic Mission (SRTM) digital elevation data (http://www2.jpl.nasa.gov/srtm/). We used N = 457 discretization cells equal to the number M of measures selected for modeling. We calculated the magnetization module for each cell using a linear inversion approach in order to obtain an equivalent source model that fits the magnetic measures. Cells magnetizations vectors were considered parallel to the present Earth's Magnetic Field. The linear inversion can be expressed in matrix form as follow:

$$F = GJ \qquad (1)$$

here F is the magnetic anomaly vector of M elements, G is the $M \times N$ matrix kernel calculated using magnetic effect for rectangular cells[25]; the matrix kernel coefficients depend on cells and measure geometry and calculate the magnetic effect of each cell over all measure stations assuming unitary magnetization; J represents the N unknown elements vector of cells magnetization. This linear system is mathematically ill-posed since potential field modeling is affected by well-known problems of algebraic ambiguity and non-uniqueness[26]. To solve this linear system is necessary to adopt a regularization algorithm. Here, we used the Levenberg–Marquardt iterative regularization minimization method[27]. This method produces solutions characterized by smooth magnetization variation between adjacent cells. We assumed that the Etna volcanic pile can be modeled by a dominant bulk magnetization; this perspective implies that the calculated solution contains information about volcanic pile thickness described through cells magnetization contrasts. To reconstruct the magnetic bottom from the calculated model, we fixed a constant magnetization reference value for all the cells; then, in order to compensate the magnetic effect change, we modified each cell thickness to maintain its contribution to the total magnetic anomaly. As a con-

sequence, it is possible to solve many nonlinear problems as there are cells instead of one nonlinear multivariable problem; for each of the N discretization cells, we calculated its thickness using the following minimization relation:

$$h_n : \rightarrow = \min_h \left[\sum_{m=1}^{M} \left(G_{m,n} - \bar{G}(h_n)_{m,n} \bar{J} \right) \right] \qquad (2)$$

$1 \leq n \leq N$;

subject to $h_n \in [min, max]$

where n represents the index of N discretization cells and m the measure station index, $G_{m,n}$ is the matrix kernel of the linear inversion cells and J_n the calculated magnetizations vector. $\bar{G}(h_n)_{m,n}$ represents the new kernel as a function of the unknown cell thickness h_n. $\bar{J}$ is the a priori fixed magnetization. We constrained the minimization problem between a minimum and maximum cell thickness ([min,max]), 10 and 4000 meters respectively. We used a direct search minimization algorithm to solve the nonlinear problem of (2); direct search is a method for solving optimization problems that does not require any information about the gradient of the objective function[28]. For our modeling we explored fixed magnetization values in the range between 5 and 13 A/m. One 556 m deep borehole (Sg6, 144 m a.s.l.[7]) located in the southern east flank of Etna did not reach the sedimentary basement, so constraining a minimum lava thickness for this area. This lava thickness is not compatible with a bulk magnetization >13 A/m; in fact, an higher value, should imply a lower lava thickness. From our modeling, we observed a minimum RMS error using a constant magnetization value of 8 A/m for the non-linear minimization. Figure S1A and B show the fitting and RMS error of the linear inversion model and of the non-linear minimization, respectively. The RMS error after nonlinear minimization is about 10% of the magnetic anomaly standard deviation.

1. Tibaldi, A. & Lagmay, A. M. F. Interaction between volcanoes and their basement. *J. Volcanol. Geotherm. Res.* **158**, 1–5 (2006).
2. Borgia, A., Delaney, P. T. & Denlinger, R. P. Spreading Volcanoes. *Earth. Planet. Sci.* **28**, 539–570 (2000).
3. Carrasco-Núñez, G. *et al.* Multiple edifice-collapse events in the Eastern Mexican Volcanic Belt: the role of sloping substrate and implications for hazard assessment. *J. Volcanol. Geotherm. Res.* **158**, 151–176 (2006).
4. Byrne, P. K. *et al.* A sagging-spreading continuum of large volcano structure. *Geology* **41**, 339–342, doi:10.1130/G33990.1 (2013).
5. Vidal, N. & Merle O. Reactivation of basement faults beneath volcanoes: a new model of flank collapse. *J. Volcanol. Geotherm. Res.* **99**, 9–26 (2000).
6. Chiocci, L. F., Coltelli, M., Bosman, A. & Cavallaro, D. Continental margin large-scale instability controlling the flank sliding of Etna volcano. *Earth Planet. Sci. Lett.* **305**, 57–64 (2011).
7. Branca, S. & Ferrara, V. The morphostructural setting of Mount Etna sedimentary basement (Italy): Implications for the geometry and volume of the volcano and its flank instability. *Tectonophysics* **586**, 46–64 (2013).
8. Branca, S., Coltelli, M. & Groppelli, G. Geological evolution of a complex basaltic stratovolcano: Mount Etna, Italy. *Ital. J. Geosci.* **130**, 306–317 (2011).
9. Bonforte, A., Guglielmino, F., Coltelli, M., Ferretti, A. & Puglisi, G. Structural assessment of Mount Etna volcano from Permanent Scatterers analysis. *Geochem. Geophys. Geosyst.* **12**, dx.doi.org/10.1029/2010GC003213 (2011).
10. Bonforte, A. & Puglisi, G. Magma uprising and flank dynamics on Mount Etna volcano, studied using GPS data (1994–1995). *J. Geophys. Res.* **108**, dx.doi.org/10.1029/2002JB001845 (2003).
11. Azzaro, R., Bonforte, A., Branca, S. & Guglielmino, F. Geometry and kinematics of the fault systems controlling the unstable flank of Etna volcano (Sicily). *J. Volcanol. Geotherm. Res.* **251**, 5–15 (2013).
12. Azzaro, R., Branca, S., Gwinner, K. & Coltelli, M. The volcano-tectonic map of Etna volcano, 1:100.000 scale: an integrated approach based on a morphotectonic analysis from high-resolution DEM constrained by geologic, active faulting and seismotectonic data. *Ital. J. Geosci.* **131**, 153–170 (2012).
13. Argnani, A., Mazzarini, F., Bonazzi, C., Bisson, M. & Isola, I. The deformation offshore of Mount Etna as imaged by multichannel seismic reflection profiles. *J. Volcanol. Geotherm. Res.* **251**, 50–64 (2013).
14. Del Negro, C.& Napoli, R. Ground and marine magnetic surveys of the lower eastern flank of Etna Volcano (Italy). *J. Volcanol. Geotherm. Res.* **114**, 357–372 (2002).
15. Speranza, F., Branca, S., Coltelli, M., D'Ajello Caracciolo, F. & Vigliotti, L. How accurate is "paleomagnetic dating"? New evidence from historical lavas from Mount Etna. *J. Geophys. Res.* **111**, dx.doi.org/10.1029/2006JB004496 (2006).
16. Ferlito, C. & Nicotra, E. The dyke swarm of Mount Calanna (Etna, Italy): an example of the uppermost portion of a volcanic plumbing system. *Bull. Volcanol.* **72**, 1191–1207 (2010).
17. Patanè, D., Barberi, G., Cocina, O., De Gori, P. & Chiarabba, C. Time-Resolved Seismic Tomography Detects Magma Intrusions at Mount Etna. *Science* **313**, 821–823 (2006).
18. Schiavone, D. & Loddo, M. 3-D density model of Mt. Etna volcano (Southern Italy). *J. Volcanol. Geotherm. Res.* **164**, 161–175 (2007).
19. Bonaccorso, A., Currenti, G. & Del Negro, C. Interaction of volcano-tectonic fault with magma storage, intrusion and flank instability: A thirty years study at Mt. Etna volcano. *J. Volcanol. Geotherm. Res.* **251**, 127–136 (2013).
20. Apuani, T., Corazzato, C., Merri, A.& Tibaldi A. Understanding Etna flank instability through numerical models. *J. Volcanol. Geotherm. Res.* **251**, 112–126 (2013).

21. Branca, S., Coltelli, M., Groppelli, G. & Lentini F. Geological map of Etna volcano, 1:50,000 scale. *Ital. J. Geosci.* **130**, 265–291 (2011).

22. Gudmundsson, A. Magma chambers: Formation, local stresses, excess pressures, and compartments. *J. Volcanol. Geotherm. Res.* **237**, 19–41 (2012).

23. Maccaferri, F., Bonafede, M. & Rivalta, M. A quantitative study of the mechanisms governing dike propagation, dike arrest and sill formation. *J. Volcanol. Geotherm. Res.* **208**, 39–50 (2011).

24. Nicolosi, I., Blanco-Montenegro, I., Pignatelli, A. & Chiappini, M. Estimating the magnetization direction of crustal structures by means of an equivalent source algorithm. *Phys. Earth Planet. Inter.* **155**, 163–169 (2006).

25. Sharma, P. *Geophysical Methods in Geology* (Elsevier, Amsterdam, 1986).

26. Blakely, R. J. *Potential Theory in Gravity and Magnetic Applications* (Cambridge University Press, New York, 1995).

27. Press, W. H., Teukolsky, S. A., Vetterling, W. T. & Flannery, B. P. *Numerical Recipes in C: The Art of Scientific Computing* (Cambridge Univ. Press, New York, 1992).

28. Powell, M. J. D. Direct search algorithms for optimization calculations. *Acta Numerica* **7**, 287–336 (1998).

Acknowledgments

Author contributions

I.N. and F.D.C. collected and elaborated the magnetic data, and wrote the Methods. G.V. and S.B. wrote the main text by merging the magnetic and geological data, and M.C. organized the survey and provided the fund opportunities. All the authors contributed to the interpretation and reviewed the manuscript. The magnetic data are at Istituto Nazionale di Geofisica e Vulcanologia, Roma, Italy.

Additional information

Supplementary information accompanies this paper at http://www.nature.com/scientificreports

Competing financial interests: The authors declare no competing financial interests.

How to cite this article: Nicolosi, I., D'Ajello Caracciolo, F., Branca, S., Ventura, G. & Chiappini, M. Volcanic conduit migration over a basement landslide at Mount Etna (Italy). *Sci. Rep.* **4**, 5293; DOI:10.1038/srep05293 (2014).